water

MDPI

Article

Effects of Patch Properties of Submerged Vegetation on Sediment Scouring and Deposition

Yantun Song [1,*], Ruixiang Liu [1], Qiong Yang [1], Jiayi Li [1], Chongfa Cai [1], Yifan Feng [1], Guiyun Huang [2,3], Rong Hao [1], Hao Li [2,3], Changhua Zhan [1] and Xiwang Wen [1]

[1] Key Laboratory of Arable Land Conservation (Middle and Lower Reaches of Yangtze River) of the Ministry of Agriculture, Soil and Water Conservation Research Centre, Huazhong Agricultural University, Wuhan 430070, China; liuaoer123@gmail.com (R.L.); yq-01@webmail.hzau.edu.cn (Q.Y.); jy_812@webmail.hzau.edu.cn (J.L.); cfcai@mail.hzau.edu.cn (C.C.); yifanfeng2001@outlook.com (Y.F.); haorong@mail.hzau.edu.cn (R.H.); m15720968225_1@163.com (C.Z.); xiwang@webmail.hzau.edu.cn (X.W.)

[2] The Rare Plant Research Institute of Yangtze River, China Three Gorges Corporation, Yichang 443000, China; huang_guiyun@ctg.com.cn (G.H.); li_hao10@ctg.com.cn (H.L.)

[3] National Engineering Research Center of Eco-Environment Protection for Yangtze River Economic Belt, Beijing 100038, China

* Correspondence: songyt@mail.hzau.edu.cn

Abstract: Vegetation plays a key role in trapping sediments and further controlling pollutants. However, few studies were conducted to clarify the erosion and deposition laws of sediments and the influence factors caused by vegetation patch properties, which is not conducive to the revelation of riverbank protection and erosion prevention. Therefore, this study investigated the change in scouring and deposition characteristics around submerged vegetation patches of nine kinds of typical configurations and their influencing factors. Vegetation patches were assembled from three vegetation densities (G/d = 0.83, 1.3, and 1.77, representing dense, medium, and sparse, respectively), and three vegetation patch thicknesses (dn = 170, 400, and 630, representing narrow, usual, and wide, respectively), to measure vegetation patch property influences. Flow velocity, scouring, and deposition characteristics under nine patches were determined by a hydraulic flume experiment, three-dimensional acoustic Doppler velocimetry (ADV), and three-dimensional laser scanner, and then ten geometry and morphology indices were measured and calculated based on the results of laser scanning. Results showed that both vegetation patch density and thickness were positively related to the turbulence kinetic energy (*TKE*) above the vegetation canopy, and only vegetation patch density was negatively related to the flow velocity above the vegetation canopy. The relation between the product of density and vegetation patch thickness and erosion area in planform (*EA*) showed a power function (R^2 = 0.644). Both density and vegetation patch thickness determined the scouring degree, but deposition location and amount did not rely on each one simply. On average, medium density showed the smallest maximum erosion length (*MEL*), *EA*, deposition area in planform (*DA*), and average deposition length (*ADL*) and a minimum of the above parameters also occurred at narrow vegetation patch thickness. The shape factor of the erosion volume (*SFEV*), the shape factor of the deposition volume (*SFDV*), *ADL*, and *MEL* of medium density and narrow thickness vegetation patch (G/d = 1.3, dn = 170) were significantly smaller than that of other types of patches. *DA* and equivalent prismatic erosion depth on the erosion area (*EPED*) were significantly linearly related (R^2 = 0.766). Consequently, most sediment was deposited close to the vegetation patch edge. It is suggested that vegetation patch thickness and density should be given to control sediment transport. In particular, natural vegetation growth changes vegetation patch density and then alters vegetation patch thickness. Management and repair need to be first considered. The results of this study shed light on riparian zone recovery and vegetation filter strip mechanism.

Keywords: submerged vegetation patch; vegetation patch density and thickness; 3D laser scanner; scouring and deposition morphology; sediment transport

Citation: Song, Y.; Liu, R.; Yang, Q.; Li, J.; Cai, C.; Feng, Y.; Huang, G.; Hao, R.; Li, H.; Zhan, C.; et al. Effects of Patch Properties of Submerged Vegetation on Sediment Scouring and Deposition. *Water* **2024**, *16*, 2144. https://doi.org/10.3390/w16152144

Academic Editor: Roberto Gaudio

Received: 2 July 2024
Revised: 26 July 2024
Accepted: 26 July 2024
Published: 29 July 2024

1. Introduction

Vegetation plays key roles in sediment trapping, pollutant controlling, and riverbank stability, especially in riparian zones and low-gradient landscape units [1–4]. Eco-morphodynamic interactions between vegetation, flow, and sediment have promptly attracted major concerns in recent decades [5–10]. The presence of riparian vegetation changes flow conditions and turbulence and further influences the transport and deposition of sediment and pollutants and the morphology of riverine zones [11,12].

Flow velocity vertical distribution with vegetation did not obey the logarithmic law and remarkably differed from flow without vegetation [13]. Vegetation decreased the flow velocity to promote the deposition of sediments [14–18]. Also, vegetation transformed flow velocity vertical distribution to perform negative feedback, which increased the erosion around vegetation and then limited plant growth [14,19–21]. Vegetation sways under vortex-induced vibration are another type of flow acceleration that promotes agitation of the water body.

Vegetated flow showed significant anisotropy of turbulence intensity [22]. The biological and mechanical features of individual plants (e.g., plant height, stiffness, tiller) altered the interaction [17,23–25]. Vegetation patches have some distinct group properties to affect interaction (e.g., vegetation patch size, density, porosity, vegetation patch thickness, submerged ratio, and sheltering effect). These properties mostly show different characteristics from individual plants. In terms of the small vegetation patch, a lot of studies have investigated the flow structures [20,26–28]. The water flow around a small vegetation patch was not fully developed, resulting in secondary flow, coherent structure, and slender erosion pits downstream [29]. The dense density of the vegetation patch abruptly reduced average flow velocity and near-bed turbulent intensity [30] and increased the flow resistance and water depth [31]. Caroppi et al. found vegetation patch drag fluctuated from 4.4 times to 0.6 because of the reconfiguration of foliage and further affected the onset of a vegetation patch-scale vortex street [32]. Przyborowski and Loboda found momentum transport varied with vegetation patch distance, height, and plant physical characteristics [33].

The vegetation patch is comprised of plants and alters bleed flow through the vegetation patches and the shear layer in the wake, which in turn affects erosion and deposition downstream of the vegetation. Around submerged flexible patches, the length and depth of the scouring hole and deposition height increased linearly with a decrease in vegetation patch density [15]. Behind dense vegetation patches, deposition was much greater than that of around the sparse type [34]. When the width of emergent vegetation patches was smaller, flow mainly formed a shear layer on the two-dimensional horizontal plane. Part of the flow deflected laterally around the vegetation patch and mixed with other flow passing through the vegetation patch. Von Karman vortex street appeared at a distance downstream of the trailing edge of the vegetation patch. And flow velocity decreased at the distance and deposition increased [15,35,36]. As the width of submerged vegetation patches was wider, flow mainly deflected in the vertical plane, creating recirculation eddies at a certain distance from the trailing edge of the vegetation patch [37]. The distance between recirculation eddies and the trailing edge of the vegetation patch significantly affected the length of the deposition location [7].

Because plants in vegetation patches interact with each other, the effect of vegetation patches on the flow field shows different results from individuals. The thickness of the vegetation patch is the exterior property to reflect complex ones. To ecological function and economic costs, engineering measures and vegetation strips of riparian bank protection or low-gradient units should be designed by appropriate density and thickness. Whether or not cluster vegetation patches with constant density perform different erosion and deposition with thickness change. Given the abovementioned issues, nine types of patches were assembled to study sediment erosion and deposition rules and their influencing factors. This study aims to (1) investigate the difference in erosion and deposition characteristics among types of vegetation patch and their 3D morphology distribution, (2) identify the

factors influencing sediment transport, and (3) clarify the relative importance of these indices to the change in morphodynamics.

2. Experimental Design and Methodology

2.1. Vegetation Patch Configuration

A PVC solid cylinder with a diameter of 0.3 cm and a height of 20 cm imitated the stem of the plant. Four PVC cylinders were bound into a plant bundle (individual plant) (Figure 1a). The vegetation patch comprised several bundles according to density and thickness. Each plant bundle was placed in the hole of the perforated plastic plate on flume and arranged in a staggered pattern. The head edge of vegetation patch was placed 4.5 m behind the straightener of flume (Figure 2).

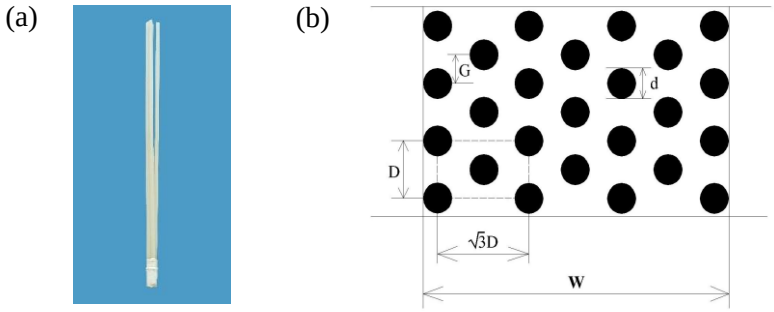

Figure 1. Configuration detail diagrams of a vegetation zone: (**a**) a PVC plant bundle and (**b**) details of vegetation patch.

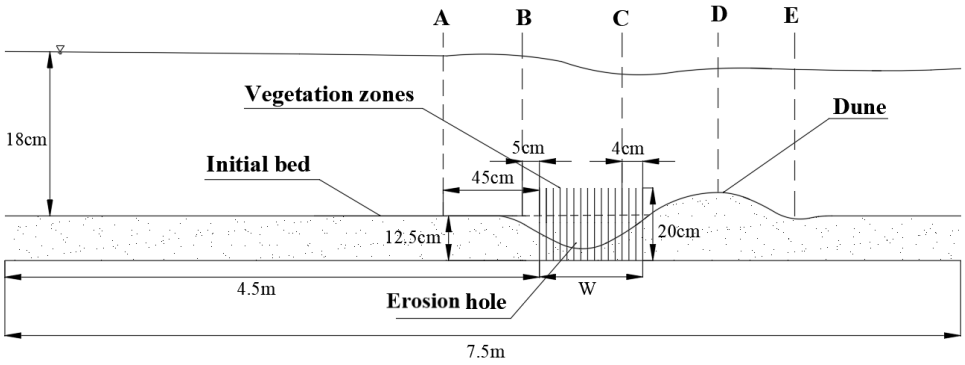

Figure 2. Schematic diagram of scouring hole and deposition dune and the location of velocity measurement (diagram is not to scale). Notes: Positions A, B, C, D, and E are, respectively, 45 cm upstream of the vegetation area, 5 cm upstream of the vegetation area, the end of the vegetation area, the highest sand accumulation downstream of the vegetation area, and the lowest sand accumulation downstream of the vegetation area. W represents the total width of the vegetation zone.

The height of vegetation patch is H (20 cm), patch density (G/d, dimensionless) set up with three values of 0.83, 1.3, and 1.77 representing dense, medium, and sparse vegetation patches, respectively (Figure 3), where G (cm) is the spanwise distance to each nearest bundle and d (cm) is the bundle diameter (Figure 1b).

Vegetation patch thickness (dn, dimensionless) is expressed as Formula (1). In this study, three thicknesses of narrow (dn_{170}), usual (dn_{400}), and wide (dn_{630}) were collected (Figure 3).

$$dn = \frac{2}{\sqrt{3}D^2}Wd \quad (1)$$

where W (cm) is the total length of each vegetation patch, D (cm) is a spanwise distance of each bundle, and d (cm) is the bundle diameter (Figures 1b and 3 and Table 1).

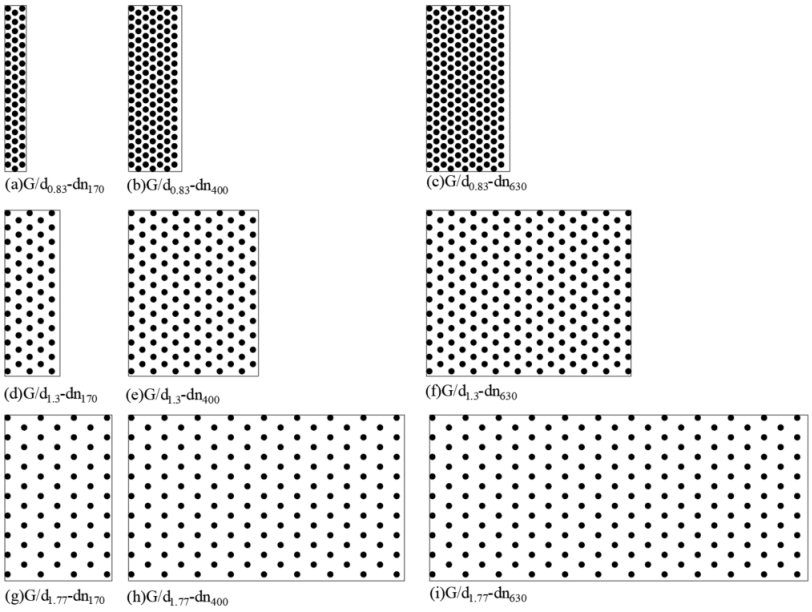

Figure 3. Schematic diagram of vegetation patch arrangement.

Table 1. Nine vegetation patch properties.

Case.	Vegetation Patch Density (G/d)	Vegetation Patch Thickness (dn)	Height (H)	Vegetation Patch Width (W)	Distance of Each Bundle (D)	Vegetation Patch Types
No.	**(-)**	**(-)**	**(cm)**	**(cm)**	**(cm)**	
1	0.83	170	20	4.0	1.66	Dense and narrow
2	0.83	400	20	9.64	1.66	Dense and usual
3	0.83	630	20	15.06	1.66	Dense and wide
4	1.30	170	20	10.00	2.60	Medium and narrow
5	1.30	400	20	23.50	2.60	Medium and usual
6	1.30	630	20	37.00	2.60	Medium and wide
7	1.77	170	20	19.39	3.54	Sparse and narrow
8	1.77	400	20	49.91	3.54	Sparse and usual
9	1.77	630	20	68.43	3.54	Sparse and wide

2.2. Sediment Bed Configuration

The flume was filled up to 12.5 cm with coarse sand obtained from riverine zone to create a flat bed. The coarse sand is a quasi-uniform sand with a median diameter D_{50} of 1 mm and a geometric standard deviation of 1.03. Under the condition of no vegetation, the critical shear velocity of the bed sediment (U_C) obtained from the Shields curve was approximately 0.36 m/s.

2.3. Morphometric Parameters Acquisition

The three-dimensional laser scanner (FARO Focus S70, FARO SINGAPORE PTE. LTD, Singapore) acquired point cloud data and the morphological features of the scouring holes and deposition around the vegetation were obtained by processing the point cloud alignment stitching, feature extraction, and vegetation data exclusion using Cloudcompare opensource software (version 2.11). The main specifications parameters of the laser scanner are shown in Table 2. The flat sand bed with vegetation patch was scanned before running the experiment. When each run lasted for 6–8 h to reach a state of equilibrium, the flow velocity measurement was initiated. Equilibrium state is considered to be reached when no difference in size of the erosion hole and deposition was observed during the 30 min interval after the 6–8 h. After each run was complete, the flume slowly dried to scan sediment bed morphology.

Table 2. Specification parameters of the Focus Series70.

Parameters	Values
Measurement distance (m)	0.6–70
Range error (mm)	±1
Measurement accuracy (mm)	0.2
Field of vision (°)	360 × 300
Laser wavelength (nm)	1550

Based on cloud points processed by 3D laser scanner, ten indices were calculated or measured to reflect erosion patterns under patches, and deposition morphology behind patches, including five erosion parameters (erosion area in planform (EA), erosion volume (EV), maximum erosion length (MEL), equivalent prismatic erosion depth on the erosion area (EPED), the shape factor of the erosion volume (SFEV)), and five deposition parameters (deposition area in planform (DA), deposition volume (DV), average deposition length (ADL), the shape factor of the deposition volume (SFDV) and the dimensionless volumetric deposition ratio (DVDR) (Table 3). Since the vegetation patches span the entire width of the flume, the width of the erosion and deposition of sediment is the width of the flume.

Table 3. Definition of morphological characteristic parameters.

Morphometric Parameter	Notes
$EPED = \frac{EV}{EA}$	EPED is the ratio of the erosion volume to the erosion area and is a length dimension. In other words, EPED expresses the equivalent prismatic erosion depth over the erosion area. This parameter quantifies the distribution of erosion affected by vegetation in the erosion area.
$SFEV = \frac{EV}{w^3}$	SFEV is the ratio of the erosion volume to the cube of the erosion width, which represents the shape of the erosion volume. SFEV quantifies the location of the erosion volume. Lower SFEV value indicates that erosion is distributed within a shorter area rather than within a longer area. w is the width of the flume.
$ADL = \frac{DA}{w}$	ADL is the ratio of deposition area to deposition width, which represents the average deposition length.
$SFDV = \frac{DV}{w^3}$	SFDV is the ratio of the deposition volume to the cube of the deposition width, which represents the shape of deposition volume. For a given deposition volume, SFDV increases with decreasing deposition length. Alternatively, for a given deposition length, the value increases with increasing deposition volume.
$DVDR = \frac{DV}{EV}$	DVDR is the ratio of the deposition volume to the erosion volume, which represents the erosion volume deposited downstream of the vegetation patch.

2.4. Hydraulic Conditions and Measurement

All experiments were carried out at the Soil and Water Conservation Laboratory at Huazhong Agricultural University in hydraulic flume. The flume is 7.2 m long, 0.3 m wide, and 0.5 m deep, and the sides and bottom of the flume are constructed of plexiglass to observe. The primary components of the flume were a head tank, electromagnetic flow meters, main channel, tail gate, tail tank, and recirculation flow system. A honeycomb flow straightener is installed at the inlet to the flume to eliminate massive turbulence and secondary flow and allow a smooth flow into the flume. The depth of flow was controlled by the tail gate. The flow in the main channel was separately controlled and measured by the discharge controlling valve and the electromagnetic flow meters. The instantaneous velocity (u_i, v_i, w_i) corresponding to the streamwise, lateral, and vertical directions, respectively, were measured by three-dimensional acoustic Doppler velocimetry (ADV) at a sampling frequency of 50 Hz. The data collection duration for each point lasted up to 5 min and each measurement point captured about 6000 data. The acceleration threshold method was employed to post-process the ADV measurement data to remove the spikes.

Flow rate of each running occurred at 0.0154 m^3/s. The uniform inlet velocity u_0 was set to 0.285 m/s, and the corresponding flow depth h reached 0.18 m. The Reynolds and Froude numbers of the inlet flow were 51,094 and 0.2, respectively.

In this experiment, an ADV instrument was applied to measure the flow velocity at each measuring point. The sampling point was located 5 cm from the head of the ADV instrument. To avoid the edge effect, acquirement flow data were arranged at the centerline of the flume. The flow velocity was measured in five vertical sections along the centerline (from location A to E) (Figure 2). Location A is located 45 cm upstream of the vegetation area. Location B is located 5 cm upstream of the vegetation area. Location C is located 4 cm at the end of the vegetation area, Location D is located at the highest sand accumulation downstream of the vegetation area, and Location E is located at the lowest sand accumulation downstream of the vegetation area. Measurements were performed at approximately 10–20 points along the vertical line, and the interval between each vertical measurement point ranged from 0.5 cm.

The mean velocity, turbulence intensity and turbulence kinetic energy are important parameters characterizing the flow structure. The instantaneous velocity (u_i, v_i, w_i) was decomposed into mean velocity (u, v, w) and fluctuation velocity (u', v', w'). Taking streamwise velocity as example, the calculation equation is as follows:

$$u = \frac{1}{n}\sum_{i=1}^{n} u_i \tag{2}$$

$$u' = u_i - u \tag{3}$$

$$u_{rms} = \sqrt{\overline{u'^2}} \tag{4}$$

where u is the mean streamwise velocity, u_i is the instantaneous streamwise velocity, u' is the fluctuation in the streamwise velocity, u_{rms} is the root mean square of the streamwise velocity, and similar for lateral and vertical directions. The time-averaged TKE, considering the turbulent intensity in three directions, can be expressed as

$$TKE = 1/2\left(u_{rms}^2 + v_{rms}^2 + w_{rms}^2\right) \tag{5}$$

3. Results

Three vegetation densities (dense, medium, and sparse) and three vegetation patch thicknesses (narrow, usual, and wide) were designed to measure vegetation patch property influences on sediment scouring and deposition. Both vegetation patch density and thickness were positively related to the TKE above the vegetation canopy, and only vegetation patch density was negatively related to the flow velocity above the vegetation canopy. Attention should be paid to the vegetation patch thickness and density characteristics controlling sediment erosion and deposition.

3.1. Flow Velocity at Different Properties of Vegetation Patch

3.1.1. Vertical Distribution of Velocity for Same Vegetation Patch Thickness and Diverse Vegetation Patch Density

The vegetation patch height (h) and uniform inlet velocity (U_0) are normalized into the vertical height and average flow velocity, respectively. The y/h =1.0 represents vegetation patch height or vegetation canopy top. The vertical distribution of the velocity of five measurement sections is illustrated in Figure 4 for the usual vegetation patch thickness (dn_{400}) and different densities.

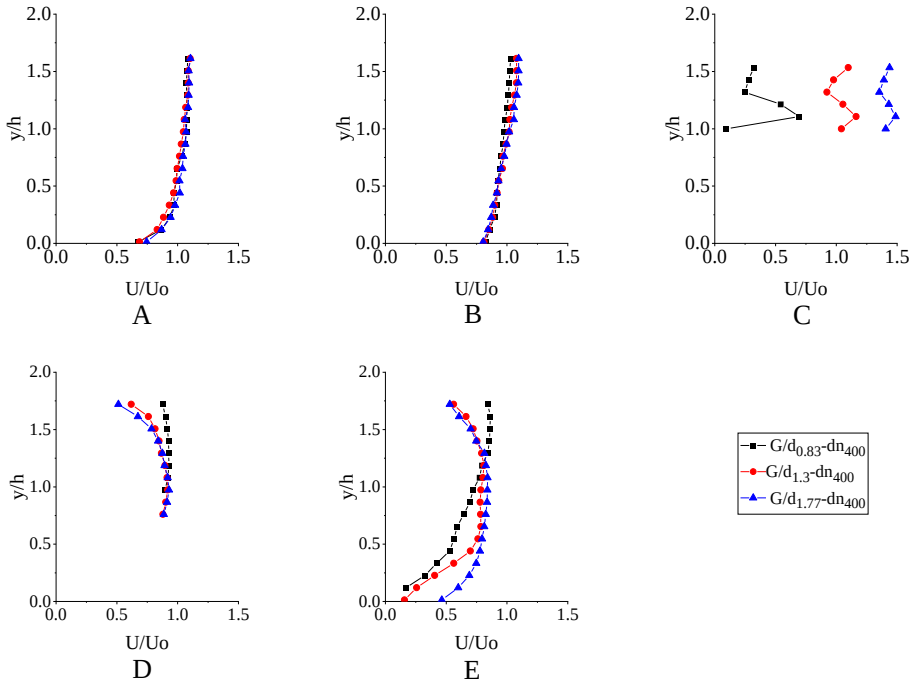

Figure 4. The vertical distribution of the normalized time average streamwise velocity at different locations with the same vegetation patch thickness and different vegetation patch densities. Note: A, B, C, D, and E are ADV five measurement vertical profiles respectively. Positions A, B, C, D, and E are, respectively, 45 cm upstream of the vegetation area, 5 cm upstream of the vegetation area, the end of the vegetation area, the highest sand accumulation downstream of the vegetation area, and the lowest sand accumulation downstream of the vegetation area.

Located 45 cm upstream of the vegetation area (location A), the vertical distribution of U/Uo under all experimental groups obeyed a log law, and the flow characteristics were consistent with fully developed flow characteristics. Located 5 cm upstream of the vegetation area (location B), the vertical distribution of the flow velocity exhibited two trends (see Figure 4). At heights of $y/h < 0.75$, the flow velocity increased with increasing vegetation patch density. With increasing vegetation patch density, the clogging effect of vegetation increased, and the flow velocity also increased. At heights of $y/h > 0.75$, the flow velocity decreased with increasing vegetation patch density. On the top of the vegetation patch (location C), due to the flow deflection of the vegetation canopy, the vertical velocity distribution first increased and then decreased and finally increased up to the free water surface. As the vegetation patch thickness remained constant, only the vegetation patch density variety resulted in increases in the flow velocity ($G/d_{1.77} > G/d_{1.3} > G/d_{0.83}$). This was consistent with the previous conclusion on the effects of vegetation patch density on flow velocity [38,39].

On top of deposition accumulation (location D), when the y/h was greater than 1.0, the velocity gradually decreased due to the disappearance of vegetation canopy vortices, and flow velocity decreased with increasing vegetation patch density ($G/d_{1.77} < G/d_{1.3} < G/d_{0.83}$). The flow velocity of the sparse vegetation patch density was slightly smaller than that of dense and medium vegetation patch density above the vegetation top and the mean deposition location of sparse vegetation patch density was closer than that of dense and medium vegetation patch density (see Figure 4). At the lowest point of the deposition dune (location E), velocity showed diverse trends. The velocity increased with increasing vegetation patch density at $y/h > 1.25$, and at $y/h < 1.25$, the flow velocity decreased with increasing vegetation patch density.

3.1.2. Vertical Distribution of Velocity for Same Vegetation Patch Density and Diverse Vegetation Patch Thickness

Located 5 cm upstream of the vegetation area (location B), when y/h was above 1.0, it was expected that the blocking effect of the usual vegetation patch thickness (dn_{400}) was the smallest. Most of the water flow passed through the vegetation zone, so the flow velocity in front of the vegetation was the lowest (see Figure 5). On the top of the vegetation canopy (location C), the velocity for the different vegetation patch thicknesses varied greatly along the vertical direction. Flow velocity showed similar variety and velocity of narrow vegetation patch thickness was minimum values, but ones of usual vegetation patch thickness were maximum values.

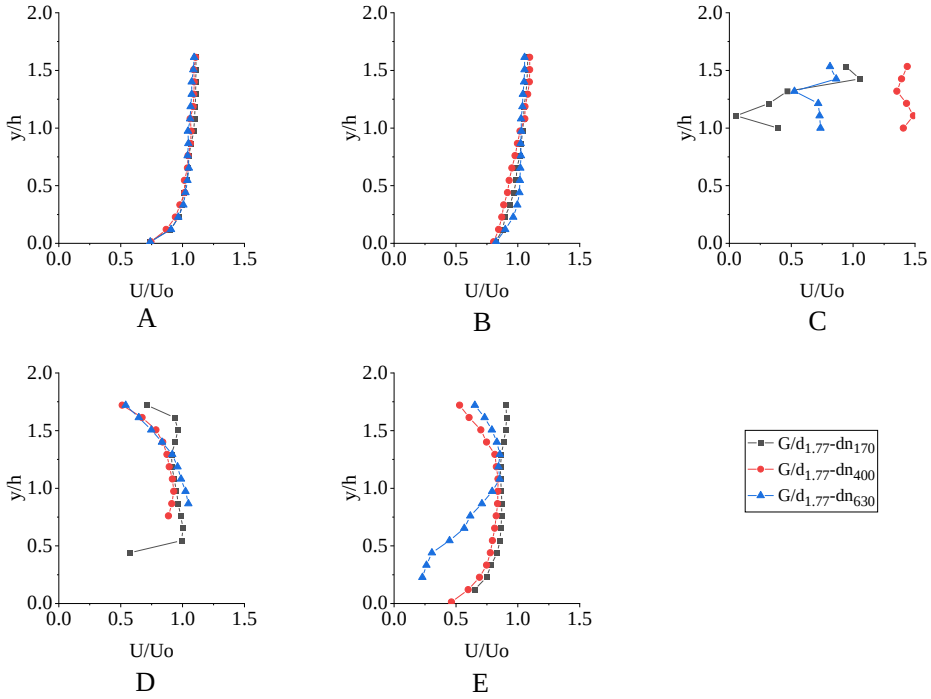

Figure 5. The vertical distribution of normalized time average flow velocity at different locations with the same vegetation patch density and different vegetation patch thicknesses. Note: A, B, C, D, and E are ADV five measurement vertical profiles respectively. Positions A, B, C, D, and E are, respectively, 45 cm upstream of the vegetation area, 5 cm upstream of the vegetation area, the end of the vegetation area, the highest sand accumulation downstream of the vegetation area, and the lowest sand accumulation downstream of the vegetation area.

On the highest deposition accumulation (location D), the velocity gradually decreased along the vertical direction. At the lowest point of the deposition dune (location E), the vertical distribution of the flow velocity exhibited two trends at y/h = 1. Below the vegetation canopy top (y/h < 1), all of the velocities gradually increased, while the flow velocity increased with decreasing vegetation patch thickness ($dn_{630} > dn_{400} > dn_{170}$). Above the vegetation canopy top (y/h > 1), the flow velocity gradually decreased except for narrow (dn_{170}) vegetation patch thickness. The vertical distribution of velocity for narrow vegetation patch thickness obeyed a log law, vegetation imposed less influence on the flow, and the flow characteristics were quickly restored. The velocity of usual vegetation patch thickness was the minimum value among the three kinds of vegetation patch thicknesses.

3.2. Characteristics of TKE at Different Properties of Vegetation Patch

3.2.1. Same Vegetation Patch Thickness and Different Vegetation Patch Density

The normalized turbulent kinetic energy for the different vegetation patch thickness and density conditions at the various locations is shown in Figure 6. The turbulent kinetic

energy is lower upstream of the vegetation area (locations A and B) far away from the sand bed. The turbulent kinetic energy values have a maximum near the sand bed layer and slightly decrease towards the water surface, similar to the trend of the TKE [40]. On the top of the vegetation canopy (location C), due to the block influence of the submerged vegetation canopy, higher TKE was produced, therefore the TKE is significantly higher than those positioned upstream.

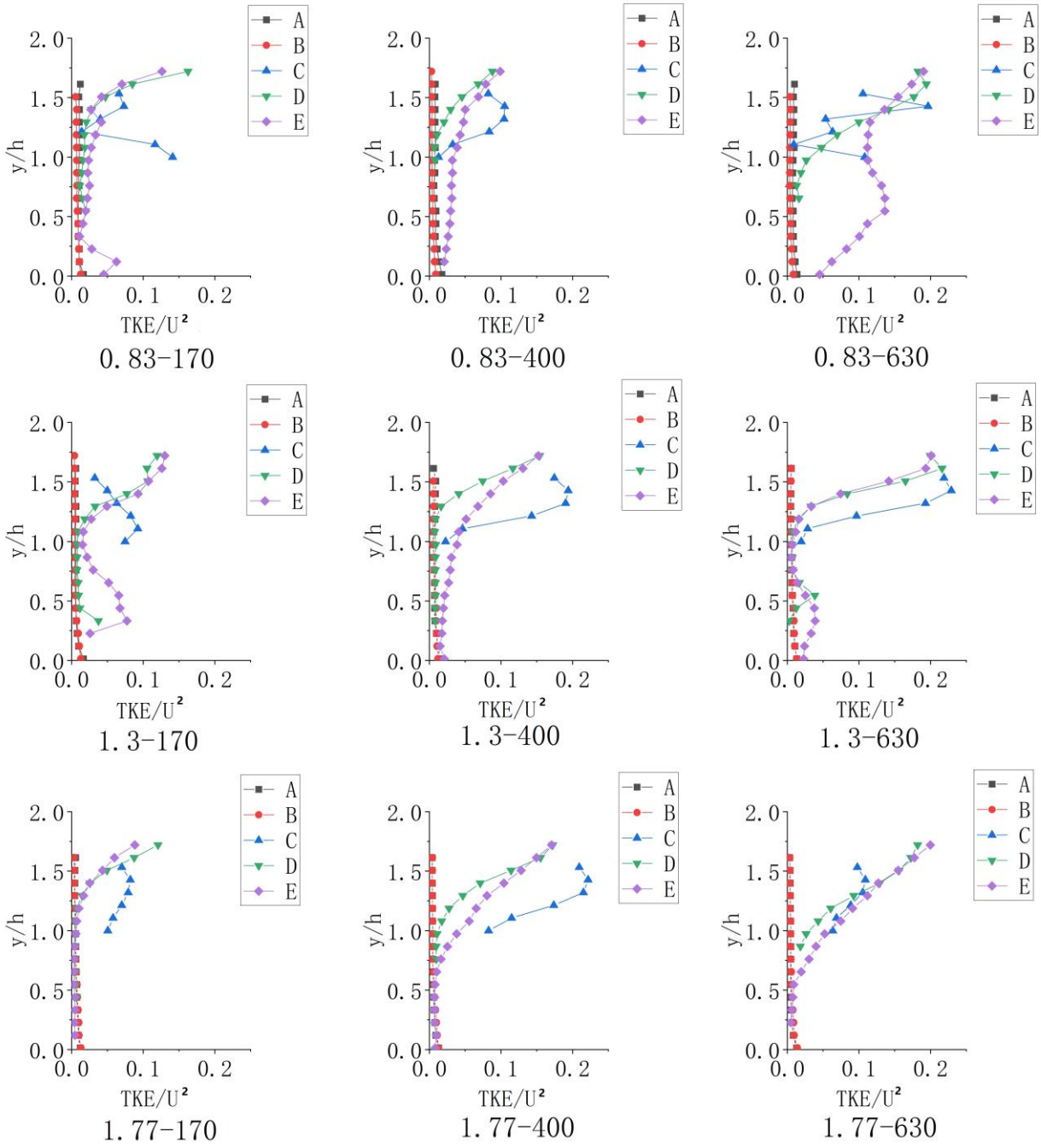

Figure 6. The vertical distribution of the normalized TKE at different locations.

On the highest deposition accumulation (location D), due to the blocking effect of vegetation and higher TKE at location C, a stable wake zone was formed near the downstream of the vegetation area. TKE of the vegetation canopy top was lower than that of $y/h > 1$. The TKE decreased with increasing vegetation patch density ($G/d_{1.77} < G/d_{1.3} < G/d_{0.83}$). On the lowest deposition accumulation (location E), the trend of TKE showed a difference

at y/h = 1.0. Below the vegetation patch height, the vegetation canopy-scale turbulence was jointly affected by deposition dune and vegetation blockage, and the TKE was lower. When y/h was greater than 1.0, the TKE increased promptly.

3.2.2. Same Vegetation Patch Density and Different Vegetation Patch Thickness

The normalized TKEs for sparse vegetation patch density and different vegetation patch thickness patches at different sections are shown in Figure 6. At the upstream of the vegetation area (locations A and B), TKE was greater near the sand bed and was lower in the zone away from the sand bed because of the roughness of the sand bed. On the top of the vegetation patch (location C), the TKE of the usual vegetation patch thickness vegetation patch was greater than that of other types. This was also consistent with the observed results of flow velocity of the same vegetation patch density and different vegetation patch thickness. Downstream of the vegetation area (locations D and E), when y/h was smaller than 0.75, the TKE was lower. While y/h was greater than 0.75, the TKE increased with increasing vegetation patch thickness ($dn_{630} > dn_{400} > dn_{170}$).

3.3. Morphology of Scouring and Deposition

Geometric and morphology indices of scouring and deposition were carried out based on a 3D laser scanner (Table 4). The morphological characteristics observed in this experiment included size-related parameters (*EA*, *DA*, *EV*, *DV*, *ADL*, and *MEL*). To better compare, proportional parameters between the geometric features were considered, including *EPED*, *DVDR*, SFDV, and *SFEV*. The scouring and deposition patterns for different densities and thicknesses are shown in Figures 7–9. The medium (G/d = 1.3) and sparse (G/d = 1.77) density of the vegetation patch showed significantly wider and shallower scouring than that of the dense one, and the deposition area of medium vegetation patch density behind the vegetation patch was restricted largely (see Figure 7). The *DVDR* (0.90) of dense vegetation patches clearly indicated that dense vegetation patches generated larger deposition than that of other types when the vegetation patch thickness remained constant (Table 4 and Figure 7). The scouring and deposition patterns for different thicknesses of sparse vegetation patch density (G/d = 1.77) are shown in Figure 8. When the vegetation patch density remained constant, scouring and deposition showed similar morphology. Vegetation patch density was the key factor that controlled scouring and deposition. At the same time, it can be seen from Table 4 that with the increase in vegetation patch thickness, SFDV and SFEV also increased, the scouring expanded, and the deposition increased. SFEV and SFDV of the wide thickness vegetation patch (dn_{630}) were 1.6–3.0 times and 2.0–3.5 times greater than those narrow vegetation patch thickness vegetation patch (dn_{170}), respectively. When vegetation patch density remained constant, *DVDR* increased with increasing vegetation patch thickness (Table 4 and Figure 8).

Table 4. Characteristics of the scouring pattern and deposition morphology.

Vegetation Patch Configuration No.	Vegetation Patch Density (-)	Vegetation Patch Thickness (-)	MEL (cm)	EA (cm^2)	EV (cm^3)	EPED (cm)	SFEV (-)	ADL (cm)	DA (cm^2)	DV (cm^3)	DVDR (-)	SFDV (-)	Product of Density and Thickness (-)
1	0.83	170	36.00	715.77	2128.83	2.97	0.08	33.54	1006.33	1627.90	0.77	0.06	141.1
2	0.83	400	42.60	1136.98	5002.53	4.40	0.19	77.78	2333.29	4491.13	0.90	0.17	332.0
3	0.83	630	44.80	1195.52	5491.11	4.59	0.20	56.27	1687.97	4808.26	0.98	0.18	522.9
4	1.30	170	20.20	446.18	485.57	1.08	0.02	9.69	290.84	303.00	0.62	0.01	221.0
5	1.30	400	31.50	785.70	1387.70	1.69	0.05	18.41	552.23	936.70	0.68	0.03	520.0
6	1.30	630	41.70	928.16	1838.14	1.98	0.07	26.20	785.99	1319.78	0.72	0.05	819.0
7	1.77	170	35.20	789.19	1844.72	2.34	0.07	28.80	863.95	1394.61	0.76	0.05	300.9
8	1.77	400	59.00	1412.99	3507.01	2.48	0.13	36.99	1109.74	2703.20	0.77	0.10	708.0
9	1.77	630	75.00	2101.07	5552.41	2.64	0.21	49.87	1496.20	4279.10	0.78	0.16	1115.1

Notes: MEL is the maximum erosion length, EA is the erosion area in planform, EV is the erosion volume, DA is the deposition area in planform, DV is the deposition volume, EPED is the equivalent prismatic erosion depth over the erosion area, SFEV is the shape factor of the erosion volume, DVDR is dimensionless volumetric deposition ratio. SFDV is the ratio of the deposition volume to the cube of the deposition width, which represents the shape of deposition volume. ADL is the ratio of deposition area to deposition width, which represents the average deposition length.

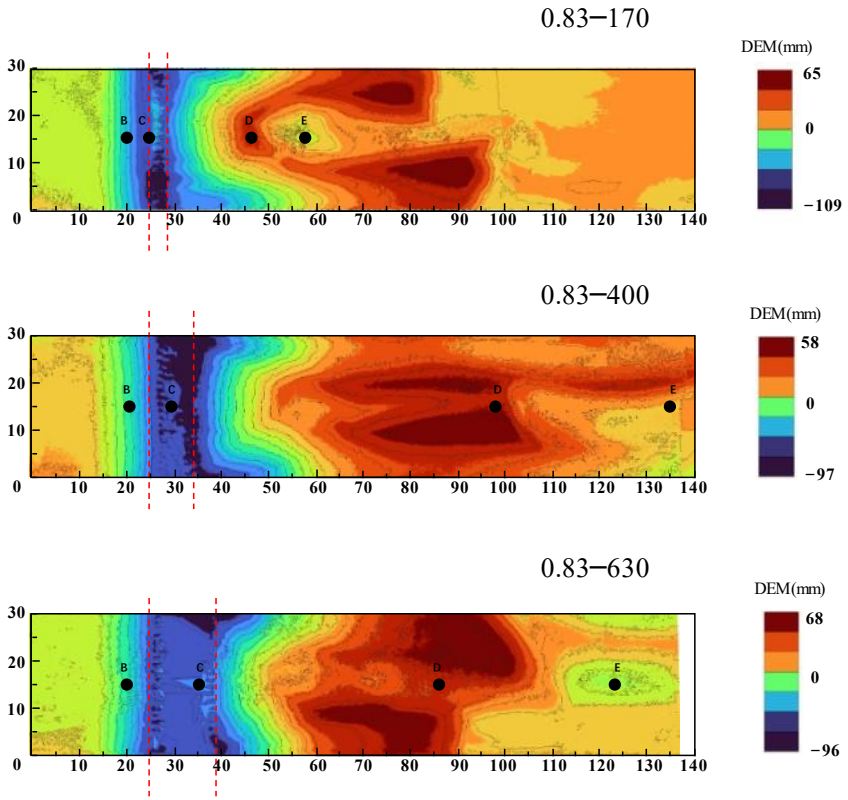

Figure 7. Erosion and deposition patterns of the same densities ($G/d_{0.83}$) and different thicknesses (170, 400, and 630, respectively). Notes: Zones between the two dotted vertical lines are the vegetation patches. B, C, D, and E are measured locations of ADV, respectively.

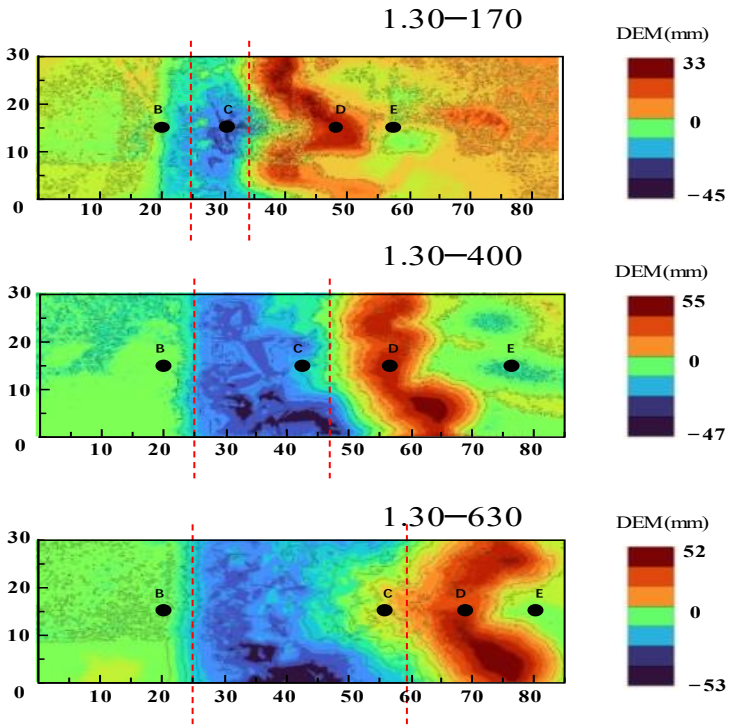

Figure 8. Erosion and deposition patterns of the same densities ($G/d_{1.30}$) and different thicknesses (170, 400, and 630, respectively). Notes: Zones between the two dotted vertical lines are the vegetation patches. B, C, D, and E are measured locations of ADV, respectively.

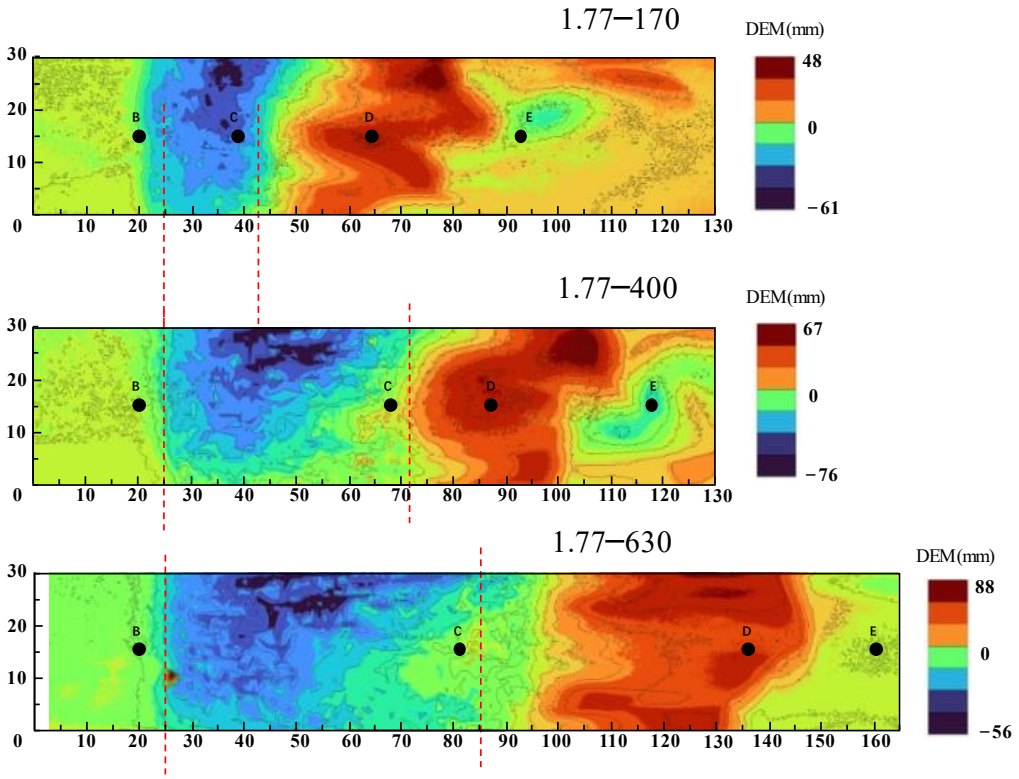

Figure 9. Erosion and deposition patterns of the same densities ($G/d_{1.77}$) and different thicknesses (170, 400, and 630, respectively). Notes: Zones between the two dotted vertical lines are the vegetation patches. B, C, D, and E are measured locations of ADV, respectively.

The relation between the product of vegetation patch density and vegetation patch thickness and *EA* showed power function ($y = 508.38e^{0.1287x}$, $R^2 = 0.644$). Both vegetation patch density and thickness determined scouring degree, but deposition location and amount did not rely on each one simply. On average, medium vegetation patch density showed *MEL*, *EA*, *DA*, and *ADL*, and a minimum of the above indices also occurred at narrow vegetation patch thickness. *SFEV*, *SFDV*, *ADL*, and *MEL* of medium vegetation patch density and narrow thickness vegetation patch ($G/d = 1.3$, $dn = 170$) were significantly smaller than those of other types of patches. *DA* and *EPED* were significantly linearly related ($y = 200.08x + 124.79$, $R^2 = 0.766$).

4. Discussion

4.1. Effect of Properties of Vegetation Patch on Hydraulic and Sediment Dynamics

This research results show that both vegetation patch density and vegetation patch thickness have affected the flow characteristics and sediment erosion and deposition around vegetation patches, and the flow velocity and turbulent kinetic energy will decrease with the increase in vegetation patch density and thickness [15,41]. However, among the three densities of vegetation patches, the erosion and deposition of medium vegetation patch density are the most local, which is consistent with the results of Ali and Tanaka [42]. Also, this study observed a low-velocity area downstream of vegetation patches with medium vegetation patch density, so less erosion was observed in the case of medium vegetation patches. The flow through medium vegetation patch density was stronger than that through high vegetation patch density, which was sufficient to suppress the formation of vortices along the longitudinal profile. Additionally, the dense vegetation patches increased the velocity gradient and vortices of vegetation canopy within the vegetation patches, thereby increasing erosion in the monitoring area, and deposition behind the vegetation patches also increased. The erosion of sparse vegetation patches is greater than that of medium vegetation patches [43]. According to Yagci et al., small-scale turbulence is generated by

cylindrical patches due to vortices, which enhances erosion in the vegetation zone [43]. In this study, sparse vegetation generated more turbulence in the patches and increased vertical mixing of recirculating vortices downstream of the vegetation patches. Hence, erosion occurred within a larger region in the monitoring area.

At the same vegetation patch density, the increase in vegetation patch thickness can significantly change the fluctuation of TKE at the top of the vegetation patch canopy and the difference of TKE along various flow depths. The 400 and 630 vegetation patch thickness of TKE show consistent patterns in Figure 6. The above results can be strongly confirmed by nine different erosion patterns of the same density and different vegetation patch thickness. At three densities (0.83, 1.30, and 1.77), the erosion areas of the usual and the wide vegetation patch thickness patches are broad, and the erosion lengths are longer than those of the narrow vegetation patch thickness plant patches, and the erosion morphologies are more complex also. The properties of vegetation patch density and vegetation patch thickness can also affect the reconfiguration characteristics of vegetation patches [25,32], which is also indirectly supported by the results of this study.

EPED, SFEV, ADL, and SFDV increase linearly with the vegetation patch thickness of vegetation patch rather than vegetation patch density. Relative to the vegetation patch thickness, the erosion and deposition characteristic parameters of different vegetation densities are quite different, and EPED, MEL, SFEV, and ADL after vegetation patches are the smallest for medium vegetation densities, which are 64%, 47%, 82%, and 65% reduction compared to other vegetation patch density conditions, respectively [10,32]. Among the factors controlling vegetation patch density and vegetation patch thickness, vegetation patch density is the main factor controlling the erosion and deposition of vegetation monitoring areas. However, under the same vegetation patch density, the vegetation patch thickness is the dominant factor controlling the erosion and deposition in the vegetation monitoring area. The dense vegetation patches increase the shear of the riverbed, thereby increasing the erosion in the vegetation monitoring area; the sparse vegetation patches generate more turbulence around the vegetation, increasing the local shear force near the riverbed, resulting in increased erosion in the vegetation monitoring area.

4.2. Ecological Implications of Properties of Vegetation Patch

For a long time, many hardened concrete berms have been built to improve the ability of rivers to withstand flooding. However, this initiative has led to a reduction in riparian biodiversity and disruption of the ecosystem balance [44]. To solve the problems caused by hard protection engineering, the construction of ecological protection works such as vegetation biobarriers is a necessary measure. Through appropriate vegetation patch placement, overall design, and management, it has the potential to provide the same level as hard protection engineering. In addition, when the ecosystem services provided by vegetated bioshields are considered, the costs of construction and preservation are obviously reduced compared to hard solutions. Dense vegetation attenuates wave intensity, properly increasing the width of the wood buffer can improve the removal efficiency of sediment and sediment nutrients [45]. Veettil's research emphasized how critical native mangroves and Casuarina trees are to Vietnam as biological barriers [46]. Therefore, selecting an appropriate vegetation patch layout can better play the role of a vegetation biological barrier.

This study demonstrates the distinctly different hydrodynamics and sediment dynamics between plant patches of different densities and thicknesses, clearly demonstrating the importance of vegetation patch characteristics such as vegetation patch density and vegetation patch thickness for riparian ecosystems. The role of vegetation as an ecological barrier depends on the characteristics of its community, as well as the location of the patches. Usually, river banks are characterized by concave bank erosion and convex bank deposition [47], which may increase the risk of flooding and affect navigation. Yang et al. showed that river stability was superior under bilateral riparian vegetation cover than unilateral vegetation [48]. Therefore, in the course of riparian management, for rivers with

a flood control and navigation role, which usually require the river to be straight [49], high vegetation patch density can be set up at the head of concave banks, while the vegetation patch thickness is as large as possible to increase the sedimentation of the concave banks. Medium vegetation patch density vegetation patches are set up at the head of convex banks, while the vegetation patch thickness is as small as possible to reduce deposition on the convex banks.

5. Conclusions

Laboratory experiments were undertaken to explore the effect of different forms of artificial vegetation patches on flow structures and sediment erosion patterns. The main conclusions are as follows. There existed a certain threshold for the distance between vegetation clusters. The flow velocity decreased, and the turbulent kinetic energy increased with increasing plant bundle spacing, which enhanced the small-scale turbulence between the sparser plant bundles and promoted turbulence and erosion around the vegetation patches. The medium vegetation patch density attained a lower flow velocity and higher turbulent kinetic energy than those yielded by the dense vegetation patch density. A reduction in between plant bundle spacing increased the mixing of the canopy and vertical vortices behind the vegetation patches, enlarging the erosion zone. With increasing vegetation patch thickness, the flow velocity decreased, the turbulent kinetic energy increased, the erosion zone expanded, and the deposition distance behind the vegetation patch increased.

Vegetation biobarriers are an important measure. Appropriate vegetation patch placement, design, and management have the potential to provide the same level as hard protection engineering. Vegetated bioshields are considered to have a clear advantage over hard solutions in terms of construction cost and protective effectiveness. River stability was superior under bilateral riparian vegetation cover than unilateral vegetation. High-density vegetation patches can be arranged at the head of concave banks, while the vegetation patch thickness is as large as possible to increase the sedimentation of the concave banks. Medium-density vegetation patches are set up at the head of convex banks, while the vegetation patch thickness is as small as possible to reduce deposition on the convex banks.

Although this study partially revealed the effects of external properties of vegetation patches on hydrodynamic characteristics and sediment deposition and erosion. The non-unidirectional flow characteristics of the natural environment and the effects of water level fluctuation are not considered in this study, which is the direction of further research in the future.

Author Contributions: Conceptualization, Y.S.; Investigation, R.H.; Resources, G.H., R.H. and H.L.; Data curation, R.L. and Q.Y.; Writing—original draft, Y.S., C.Z. and X.W.; Writing—review & editing, Y.S., J.L., C.C., Y.F., G.H. and R.H.; Supervision, Y.S.; Funding acquisition, Y.S. All authors have read and agreed to the published version of the manuscript.

Funding: This work has been supported by the National Natural Science Foundation of China (U2240222 and 41471432) and the National Key Research and Development Program of China (2021YFD1500703).

Data Availability Statement: Data are contained within the article.

Acknowledgments: The authors would like to thank all the referees for providing their helpful and constructive comments.

Conflicts of Interest: Authors Guiyun Huang and Hao Li were employed by the Rare Plant Research Institute of Yangtze River, China Three Gorges Corporation. The remaining authors declare that the research was conducted in the absence of any commercial or financial relationships that could be construed as a potential conflict of interest.

References

1. Afzalimehr, H.; Dey, S. Influence of bank vegetation and gravel bed on velocity and Reynolds stress distributions. *Int. J. Sediment Res.* **2009**, *24*, 236–246. [CrossRef]

2. McMahon, J.M.; Olley, J.M.; Brooks, A.P.; Smart, J.C.R.; Stewart-Koster, B.; Venables, W.N.; Curwen, G.; Kemp, J.; Stewartd, M.; Saxton, N.; et al. Vegetation and longitudinal coarse sediment connectivity affect the ability of ecosystem restoration to reduce riverbank erosion and turbidity in drinking water. *Sci. Total Environ.* **2020**, *707*, 135904. [CrossRef] [PubMed]
3. Sandjensen, K.; Madsen, T.V. Patch Dynamics of the Stream Macrophyte, Callitriche-Cophocarpa. *Freshw. Biol.* **1992**, *27*, 277–282. [CrossRef]
4. Schulz, M.; Kozerski, H.P.; Pluntke, T.; Rinke, K. The influence of macrophytes on sedimentation and nutrient retention in the lower River Spree (Germany). *Water Res.* **2003**, *37*, 569–578. [CrossRef] [PubMed]
5. Anjum, N.; Tanaka, N. Investigating the turbulent flow behaviour through partially distributed discontinuous rigid vegetation in an open channel. *River Res. Appl.* **2020**, *36*, 1701–1716. [CrossRef]
6. Gurnell, A.M.; Bertoldi, W.; Corenblit, D. Changing river channels: The roles of hydrological processes, plants and pioneer fluvial landforms in humid temperate, mixed load, gravel bed rivers. *Earth-Sci. Rev.* **2012**, *111*, 129–141. [CrossRef]
7. Hu, Z.H.; Lei, J.R.; Liu, C.; Nepf, H. Wake structure and sediment deposition behind models of submerged vegetation with and without flexible leaves. *Adv. Water Resour.* **2018**, *118*, 28–38. [CrossRef]
8. Nepf, H.M. Flow and Transport in Regions with Aquatic Vegetation. *Annu. Rev. Fluid Mech.* **2012**, *44*, 123–142. [CrossRef]
9. Soler, M.; Colomer, J.; Folkard, A.; Serra, T. Particle size segregation of turbidity current deposits in vegetated canopies. *Sci. Total Environ.* **2020**, *703*, 134784. [CrossRef]
10. Zen, S.; Perona, P. Biomorphodynamics of river banks in vegetated channels with self-formed width. *Adv. Water Resour.* **2020**, *135*, 103488. [CrossRef]
11. Le Bouteiller, C.; Venditti, J.G. Sediment transport and shear stress partitioning in a vegetated flow. *Water Resour. Res.* **2015**, *51*, 2901–2922. [CrossRef]
12. Li, X.; Huang, L.; Reible, D.; Zeng, X.; Liu, S.; Fu, J.; Wang, K.; Fang, H. Inhibition of sediment erosion and phosphorus release by remediation strategy of contaminated sediment backfilling. *Water Res.* **2023**, *239*, 120055. [CrossRef] [PubMed]
13. Biggs, H.J.; Nikora, V.I.; Gibbins, C.N.; Cameron, S.M.; Papadopoulos, K.; Stewart, M.; Fraser, S.; Vettori, D.; Savio, M.; O'Hare, M.T.; et al. Flow interactions with an aquatic macrophyte: A field study using stereoscopic particle image velocimetry. *J. Ecohydraulics* **2019**, *4*, 113–130. [CrossRef]
14. Calvani, G.; Carbonari, C.; Solari, L. Stability Analysis of Submerged Vegetation Patterns in Rivers. *Water Resour. Res.* **2022**, *58*, e2021WR031901. [CrossRef]
15. Chen, S.C.; Chan, H.C.; Li, Y.H. Observations on flow and local scour around submerged flexible vegetation. *Adv. Water Resour.* **2012**, *43*, 28–37. [CrossRef]
16. Kothyari, U.C.; Hashimoto, H.; Hayashi, K. Effect of tall vegetation on sediment transport by channel flows. *J. Hydraul. Res.* **2009**, *47*, 700–710. [CrossRef]
17. Nepf, H.M. Drag, turbulence, and diffusion in flow through emergent vegetation. *Water Resour. Res.* **1999**, *35*, 479–489. [CrossRef]
18. Shahmohammadi, R.; Afzalimehr, H.; Sui, J.Y. Impacts of turbulent flow over a channel bed with a vegetation patch on the incipient motion of sediment. *Can. J. Civil. Eng.* **2018**, *45*, 803–816. [CrossRef]
19. Rietkerk, M.; Van de Koppel, J. Regular pattern formation in real ecosystems. *Trends Ecol. Evol.* **2008**, *23*, 169–175. [CrossRef] [PubMed]
20. Vandenbruwaene, W.; Temmerman, S.; Bouma, T.J.; Klaassen, P.C.; de Vries, M.B.; Callaghan, D.P.; van Steeg, P.; Dekker, F.; van Duren, L.A.; Martini, E.; et al. Flow interaction with dynamic vegetation patches: Implications for biogeomorphic evolution of a tidal landscape. *J. Geophys. Res.-Earth Surf.* **2011**, *116*, F01008. [CrossRef]
21. Zong, L.J.; Nepf, H. Spatial distribution of deposition within a patch of vegetation. *Water Resour. Res.* **2011**, *47*, W03516. [CrossRef]
22. Chen, S.C.; Kuo, Y.M.; Li, Y.H. Flow characteristics within different configurations of submerged flexible vegetation. *J. Hydrol.* **2011**, *398*, 124–134. [CrossRef]
23. Nepf, H.M.; Vivoni, E.R. Flow structure in depth-limited, vegetated flow. *J. Geophys. Res.-Ocean.* **2000**, *105*, 28547–28557. [CrossRef]
24. Wang, H.; Tang, H.W.; Zhao, H.Q.; Zhao, X.Y.; Lü, S.Q. Incipient motion of sediment in presence of submerged flexible vegetation. *Water Sci. Eng.* **2015**, *8*, 63–67. [CrossRef]
25. Marjoribanks, T.I.; Paul, M. Modelling flow-induced reconfiguration of variable rigidity aquatic vegetation. *J. Hydraul. Res.* **2022**, *60*, 46–61. [CrossRef]
26. Meire, D.W.S.A.; Kondziolka, J.M.; Nepf, H.M. Interaction between neighboring vegetation patches: Impact on flow and deposition. *Water Resour. Res.* **2014**, *50*, 3809–3825. [CrossRef]
27. Yagci, O.; Kabdasli, M.S. The impact of single natural vegetation elements on flow characteristics. *Hydrol. Process.* **2008**, *22*, 4310–4321. [CrossRef]
28. Yagci, O.; Tschiesche, U.; Kabdasli, M.S. The role of different forms of natural riparian vegetation on turbulence and kinetic energy characteristics. *Adv. Water Resour.* **2010**, *33*, 601–614. [CrossRef]
29. Yagci, O.; Celik, M.F.; Kitsikoudis, V.; Ozgur Kirca, V.S.; Hodoglu, C.; Valyrakis, M.; Duran, Z.; Kaya, S. Scour patterns around isolated vegetation elements. *Adv. Water Resour.* **2016**, *97*, 251–265. [CrossRef]
30. De Serio, F.; Ben Meftah, M.; Mossa, M.; Termini, D. Experimental investigation on dispersion mechanisms in rigid and flexible vegetated bed. *Adv. Water Resour.* **2018**, *120*, 98–113. [CrossRef]

31. Baptist, M.J.; Babovic, V.; Uthurburu, J.R.; Keijzer, M.; Uittenbogaard, R.E.; Mynett, A.; Verwey, A. On inducing equations for vegetation resistance. *J. Hydraul. Res.* **2007**, *45*, 435–450. [CrossRef]
32. Caroppi, G.; Vastila, K.; Jarvela, J.; Lee, C.; Ji, U.; Kim, H.S.; Kim, S. Flow and wake characteristics associated with riparian vegetation patches: Results from field-scale experiments. *Hydrol. Process.* **2022**, *36*, e14506. [CrossRef]
33. Przyborowski, L.; Loboda, A.M. Identification of coherent structures downstream of patches of aquatic vegetation in a natural environment. *J. Hydrol.* **2021**, *596*, 126123. [CrossRef]
34. Bouma, T.J.; van Duren, L.A.; Temmerman, S.; Claverie, T.; Blanco-Garcia, A.; Ysebaert, T.; Herman, P.M.J. Spatial flow and sedimentation patterns within patches of epibenthic structures: Combining field, flume and modelling experiments. *Cont. Shelf Res.* **2007**, *27*, 1020–1045. [CrossRef]
35. Chen, Z.B.; Jiang, C.B.; Nepf, H. Flow adjustment at the leading edge of a submerged aquatic canopy. *Water Resour. Res.* **2013**, *49*, 5537–5551. [CrossRef]
36. Zong, L.J.; Nepf, H. Vortex development behind a finite porous obstruction in a channel. *J. Fluid Mech.* **2012**, *691*, 368–391. [CrossRef]
37. Folkard, A.M. Hydrodynamics of model *Posidonia oceanica* patches in shallow water. *Limnol. Oceanogr.* **2005**, *50*, 1592–1600. [CrossRef]
38. Wolski, K.; Tymiński, T. Studies on the threshold density of *Phragmites australis* plant concentration as a factor of hydraulic interactions in the riverbed. *Ecol. Eng.* **2020**, *151*, 105822. [CrossRef]
39. Liu, M.Y.; Huai, W.X.; Yang, Z.H.; Zeng, Y.H. A genetic programming-based model for drag coefficient of emergent vegetation in open channel flows. *Adv. Water Resour.* **2020**, *140*, 103582. [CrossRef]
40. Zhang, Y.; Lai, X.; Jiang, J. The impact of plant morphology on flow structure: Comparative analysis of two types of submerged flexible macrophyte. *Hydrol. Sci. J.* **2016**, *61*, 2226–2236. [CrossRef]
41. Liu, C.; Nepf, H. Sediment deposition within and around a finite patch of model vegetation over a range of channel velocity. *Water Resour. Res.* **2016**, *52*, 600–612. [CrossRef]
42. Ali, A.; Tanaka, N. Experimental study of scouring downstream of coastal vegetation in an inundating tsunami current. *Landsc. Ecol. Eng.* **2020**, *16*, 273–287. [CrossRef]
43. Yagci, O.; Yildirim, I.; Celik, M.F.; Kitsikoudis, V.; Duran, Z.; Kirca, V.S.O. Clear water scour around a finite array of cylinders. *Appl. Ocean Res.* **2017**, *68*, 114–129. [CrossRef]
44. Landry, J.B.; Golden, R.R. In Situ Effects of Shoreline Type and Watershed Land Use on Submerged Aquatic Vegetation Habitat Quality in the Chesapeake and Mid-Atlantic Coastal Bays. *Estuar. Coast.* **2018**, *41*, 101–113. [CrossRef]
45. Lee, K.H.; Isenhart, T.M.; Schultz, R.C. Sediment and nutrient removal in an established multi-species riparian buffer. *J. Soil Water Conserv.* **2003**, *58*, 1–8.
46. Veettil, B.K.; Ward, R.D.; Dung, N.T.K.; Van, D.D.; Quang, N.X.; Hoai, P.N.; Hoang, N.D. The use of bioshields for coastal protection in Vietnam: Current status and potential. *Reg. Stud. Mar. Sci.* **2021**, *47*, 101945. [CrossRef]
47. Blanckaert, K.; de Vriend, H.J. Meander dynamics: A nonlinear model without curvature restrictions for flow in open-channel bends. *J. Geophys. Res.* **2010**, *115*, F04011. [CrossRef]
48. Yang, S.; Bai, Y.; Xu, H. Experimental Analysis of River Evolution with Riparian Vegetation. *Water* **2018**, *10*, 1500. [CrossRef]
49. Gao, C.; Liu, J.; Wang, Z.W. An Ecological Flood Control System in Phoenix Island of Huzhou, China: A Case Study. *Water* **2013**, *5*, 1457–1471. [CrossRef]